JOURNAL OF APPLIED PHYSICS VOLUME 89, NUMBER 12 15 JUNE 2001

Spectroscopic properties of nitrogen doped hydrogenated amorphous carbon films grown by radio frequency plasma-enhanced chemical vapor deposition

Y. Hayashi[a)]
Department of Environmental Technology and Urban Planning, Nagoya Institute of Technology, Gokiso-cho, Showa-ku, Nagoya 466-8555, Japan

G. Yu, M. M. Rahman, and K. M. Krishna
Research Center for Microstructure Devices, Nagoya Institute of Technology, Gokiso-cho, Showa-ku, Nagoya 466-8555, Japan

T. Soga and T. Jimbo
Department of Environmental Technology and Urban Planning, Nagoya Institute of Technology, Gokiso-cho, Showa-ku, Nagoya 466-8555, Japan

M. Umeno
Department of Electrical and Computer Engineering, Nagoya Institute of Technology, Gokiso-cho, Showa-ku, Nagoya 466-8555, Japan

(Received 11 December 2000; accepted for publication 19 March 2001)

Nitrogen doped hydrogenated amorphous carbon thin films have been deposited by rf plasma-enhanced chemical vapor deposition using CH_4 as the source of carbon and with different nitrogen flow rates (N_2/CH_4 gas ratios between 0 and 3), at 300 K. The dependence modifications of the optical and the structural properties on nitrogen incorporation were investigated using different spectroscopic techniques, such as, Raman spectroscopy, Fourier transform infrared spectroscopy, x-ray photoelectron spectroscopy, ultraviolet-visible (UV-VIS) spectroscopy, electron spin resonance (ESR), photoluminescence (PL) and spectroscopic ellipsometry (SE). Raman spectroscopy and IR absorption reveal an increase in sp^2-bonded carbon or a change in sp^2 domain size with increasing nitrogen flow rate. It is found that the configuration of nitrogen atoms incorporated into an amorphous carbon network gradually changes from nitrogen atoms surrounded by three (σ bonded) to two (π bonded) neighboring carbons with increasing nitrogen flow rate. Tauc optical gap is reduced from 2.6 to 2.0 eV, and the ESR spin density and the peak-to-peak linewidth increase sharply with increasing nitrogen flow rate. Excellent agreement has been found between the measured SE data and modeled spectra, in which an empirical dielectric function of amorphous materials and a linear void distribution along the thickness have been assumed. The influence of nitrogen on the electronic density of states is explained based on the optical properties measured by UV-VIS and PL including nitrogen lone pair band. © *2001 American Institute of Physics.*
[DOI: 10.1063/1.1371268]

I. INTRODUCTION

Amorphous carbon films with and without hydrogen (*a*-C:H, *a*-C, or *ta*-C) have attracted a great deal of interest for electronic and photonic devices.[1,2] These films have a number of useful properties such as high Young's modulus, high dielectric strength, chemical stability, tunable band gap by adjusting sp^2 and sp^3 bonding ratio, and high room temperature photoluminescence efficiency.[3] Moreover, amorphous carbon has attracted attention as a cheap and environmentally benign material over the hydrogenated amorphous Si (*a*-Si:H) because carbon can be produced from various sources including the natural source unlike Si, where the toxic SiH_4 is used as a source gas. Therefore, *a*-C:H films have potential technological application in fabrication of various semiconductor devices, such as, diodes, thin film transistors, solar cells, cold cathodes, or light emitting diodes.[4]

The development of a high efficiency *a*-C:H based solar cell, which is our primary target device, like hydrogenated amorphous Si (*a*-Si:H) based solar cell, has been regarded as promising for future solar power plants since it can be fabricated at a low cost on a large substrate.[4,5] Application of amorphous carbon (*a*-C) for solar cells has already been reported by various groups including ours, using different film deposition techniques.[4–8] However, realization of amorphous carbon films for semiconductor device application is still limited. The problems are high density of defects due to the complex sp^2/sp^3 mixed structure and the difficulties in controlling the conduction type, carrier concentration, and simultaneous control over optical band gap energy. Considering the widespread application of *a*-C:H, the control of doping, *p*- and *n*-type, as well as the optical band gap, re-

[a)]Electronic mail: yhayashi@theo.elcom.nitech.ac.jp

Downloaded 23 Aug 2010 to 133.68.192.97. Redistribution subject to AIP license or copyright; see http://jap.aip.org/about/rights_and_permissions

sidual defects, and chemical bonding must be achieved to realize high-performance electrical and optical devices.[9]

Although the material properties of nitrogen doped *a*-C or *a*-C:H grown by various deposition techniques have been studied by many researchers,[10–12] there has been no simultaneous study of the optical properties, nature of bonding structure, and defect states. In this article, we report the optical and microstructural properties/modifications of the nitrogen doped *a*-C:H films prepared by the rf plasma-enhanced chemical vapor deposition (PECVD) with the aim of using them in an electronic device, such as a solar cell.

II. EXPERIMENT

A parallel-plate rf PECVD reactor, using a capacitively coupled parallel plate, operating at 13.56 MHz was used to deposit *a*-C:H films on single crystal silicon (100) and electron spin resonance (ESR)-grade quartz substrates at 300 K by water cooling of the sample holder. These substrates were subjected to a HF cleaning before loading into the chamber. No bias voltage was intentionally applied between the substrate holder and the chamber wall and the low rf dc self-bias was induced between the plasma and the substrate. The rf power and the base pressure were fixed at 100 W (0.29 W/cm^2) and 10 Pa, respectively. The flow rate of CH_4 was constant at 30 sccm while that of N_2 was varied from 0 to 90 sccm (N_2/CH_4 gas ratios were between 0 and 3). The growth rate of these films measured by a step profilometer changed between 6 to 9 nm/min depending on the nitrogen flow rate for the same deposition time.

Analytical tools such as Raman spectroscopy. Fourier transform infrared (FTIR) spectroscopy, x-ray photoelectron spectroscopy (XPS), UV-visible (UV-VIS) spectroscopy, spectroscopic ellipsometry (SE), ESR, and photoluminescence (PL) were employed to investigate how the nitrogen flow rate/concentration changes the optical properties, structure, and defect states.

The Raman spectra were measured in the back-scattering geometry with the 514.5 nm line of an Ar^+ ion laser at room temperature in the spectral range from 900 to 1800 cm^{-1} with a resolution of 2 cm^{-1}, and the signals were separated by a monochromator.

FTIR absorbance spectra were recorded with a resolution of 4 cm^{-1} and scanned 600 times at room temperature in order to compare the Raman spectra and know the bonding configuration.

For the analysis of bonding configurations in the amorphous network, XPS measurements were carried out using Al K_α radiation ($h\nu = 1486.6$ eV) with 600 μm spot size. The XPS spectra for the films were obtained after a sputter cleaning using 1.5 keV Ar^+ ion beam for 10 s in order to remove surface contaminants. It is well know that Ar^+ ion sputtering of C–N films modifies their composition due to a preferential sputtering of nitrogen atoms. In our experiments, we observed no compositional change of the films by Ar^+ ion sputtering with beam energies up to 3.0 keV.

Room temperature reflectance (R) and transmittance (T) measurements were performed by UV-VIS spectrophotometer (JASCO V-570), and the absorption coefficient $[\alpha(E)]$ as a function of photon energy (E) and optical band gap were obtained from R and T.

TABLE I. Summary of deposition conditions and nitrogen concentration obtained by XPS for nitrogen doped *a*-C:H films grown by rf PECVD.

Sample No.	N_2(sccm): CH_4(sccm)	XPS (at. %)
1	0:30	0.0
2	10:30	4.6
3	30:30	6.8
4	60:30	8.8
5	90:30	21.2

The measurements of SE were carried out at an angle of incidence of 70° in the wavelength range of 300–830 nm. The SE used was of the rotating analyzer type, fitted with a 75 W xenon lamp as a light source. The optical properties of the thin films were fitted directly to measured SE (Δ, Ψ) data using empirical dielectric function. All the measurements were performed at room temperature.

The paramagnetic defect density of the samples was measured using an *X*-band (9.5 GHz) ESR spectrometer equipped with liquid–helium (4.2 K) measurement capability. A 100 KHz modulation of microwave intensity was used and a Mn^{2+} reference was used to evaluate the g value and spin density of a paramagnetic center.

PL measurements were done with a 2.4 W/cm^2 excitation density 325 nm line of He–Cd laser at room temperature. The PL signals were dispersed by a monochromator and were detected by a photomultiplier tube using ''lock-in'' technique.

III. RESULTS AND DISCUSSION

The film deposition conditions and the nitrogen concentration present in the film measured by XPS are summarized in Table I. The nitrogen concentration varies up to a maximum of 21.2 at.% as the nitrogen flow rate is increased to 90 sccm.

Figure 1 shows the Raman spectra of nitrogen doped

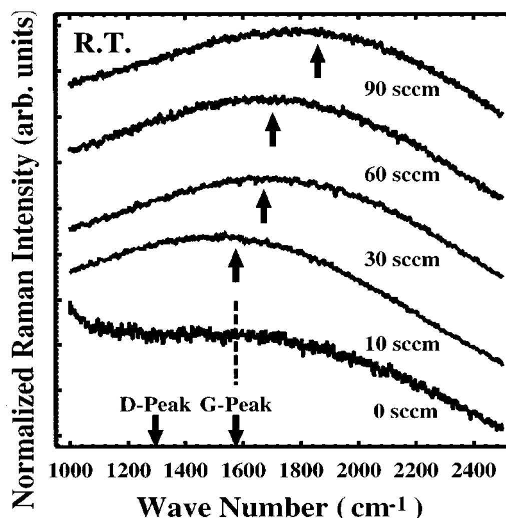

FIG. 1. First order Raman spectra of rf PECVD grown nitrogen doped *a*-C:H films with different nitrogen flow rates.

Downloaded 23 Aug 2010 to 133.68.192.97. Redistribution subject to AIP license or copyright; see http://jap.aip.org/about/rights_and_permissions

a-C:H films deposited with different nitrogen flow rates. The two distinct *D* (at around 1300 cm^{-1}) and *G* (at around 1590 cm^{-1}) peaks, commonly observed for *a*-C, are not observed in our samples; rather, a broad band with gradually increasing peak intensity at around 1600–1800 cm^{-1} is observed. The peak is found to shift towards the higher frequency without any increase in intensity upon increasing the nitrogen flow rate above 30 sccm indicating an increase of sp^2-bounded carbon in our films.[9] The position of the *G* peak is complicated and depends on the local environment of the benzene clusters and sp^2 bonding.[13] The detailed reason why the peaks shift across the *G* peak for the films deposited at higher flow rates of nitrogen is not clear at this time; however, this may be attributed to the large change in the size of the sp^2 carbon domain, the overlap of a C═N band,[14] or the characteristics of a triple N—C stretch instead of single bonding (≃2140 cm^{-1}) and/or N^{2+} structure (≃2240 cm^{-1}).[15]

In general, FTIR absorptions form a very broad band involving C—C, C—N, and C═C contributions which are difficult to distinguish. The FTIR spectra show that there are two broad absorption bands between 1200 and 1600 cm^{-1} peaking at around 1350 and 1570 cm^{-1}, respectively, as shown in Fig. 2(a). The background signal of the spectra may be due to the large amount of hydrogen in the films. These two bands correspond to Raman *G* and *D* bands, respectively, which are not observed in the Raman spectra. Raman *G* and *d* bands are normally IR forbidden, however, since the incorporated nitrogen atoms in sp^2 carbon cluster breaks the symmetry of the sp^2 domains,[14] the Raman active *G* and *D* bands also become IR active. The exact reason why we observe clear *G* and *D* bands only by FTIR and not by Raman spectroscopy is not clear, however, this may be due to the presence of a large amount of hydrogen in the films. The presence of these bands clearly indicates that the nitrogen atom is effectively incorporated into the amorphous carbon network. The feature around 1740 cm^{-1} for the films deposited with 0 and 60 sccm N_2 flow rate may arise from benzene related stretching.[16] We observe new broad absorption band at around 1610 cm^{-1} for the film deposited with the highest nitrogen flow rate (=90 sccm). This peak may be due to the C═C sp^2 stretching vibrations of the olefinic or conjugated carbon chains (or first-order scattering from features in the density states of a graphite network).[17] This indicates an increase in sp^2-bonded carbon or a change in sp^2 domain size in our films with increasing nitrogen flow rate. Figure 2(b) shows the FTIR spectrum of the film deposited with 60 sccm N_2 flow. The absorption of CH stretching around 2950 cm^{-1} can be separated into three peaks centered at 2875, 2935, and 2965 cm^{-1}. The peaks centered at 2875 and 2935 cm^{-1} are assigned to a sp-CH_n vibration mode, while that at 2965 cm^{-1} is assigned to both sp^3 and sp^2 CH vibration modes.[18] The absorption between 3000 and 3250 cm^{-1} corresponds to the vibration of CH_2, NH_2, and CH bonds, whereas the strong absorption between 3200 and 3500 cm^{-1} mostly indicates the presence of NH bonds.[19,20] This result also supports our aforementioned assumption of the presence of hydrogen in the films.

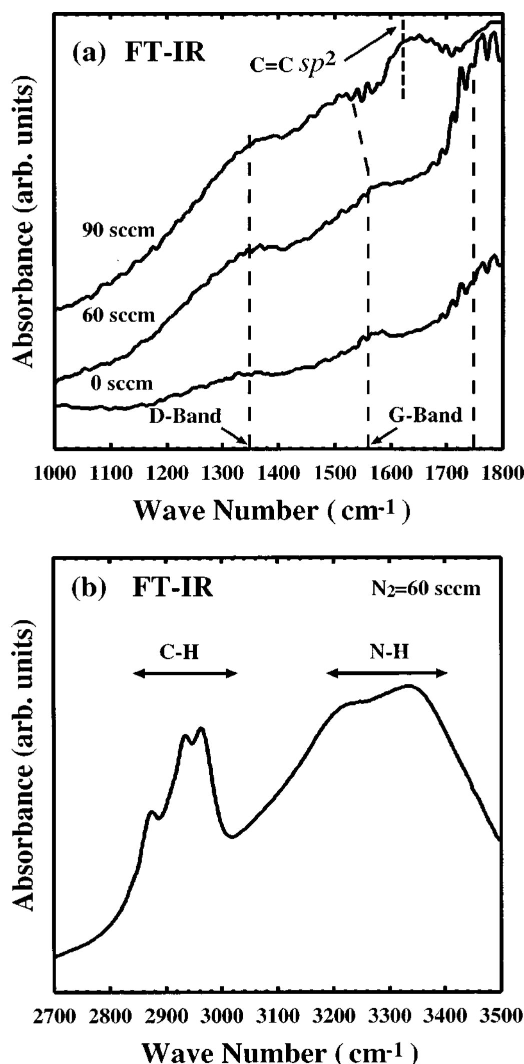

FIG. 2. FTIR spectra of rf PECVD grown nitrogen doped *a*-C:H films with different nitrogen flow rates (a). FTIR spectrum of the film grown with 60 sccm nitrogen flow over the wave number range 2700–3500 cm^{-1} (b).

The XPS N_{1s} core-level spectra of nitrogen doped *a*-C:H films are shown in Fig. 3 The XPS data can be analyzed quantitatively using a computer to reproduce the data as a sum of bands with the 100% Gaussian line shape. The N_{1s} spectra are composed of three states, centered at around 398.6 eV (N1), 400.5 eV (N2), and 403.5 eV (N3). The broad band N3 is attributed to residual oxygen contamination resulting in N—O bonds due to exposure to the atmosphere. Based on the theoretical works of Sitch[21] and Stumm,[22] there are three possible configurations in which the nitrogen atoms incorporated into *a*-C:H are surrounded by one, two, or three neighbor carbon atoms.[23] Single neighbor (C≡N) bonding configuration can be excluded from our samples due to its minor role in C—N network,[24,25] and also there is no evidence that a large fraction of C≡N bonds is present in the material as has been observed from FTIR spectra. Therefore, the peaks N1 and N2 are attributed to nitrogen atoms surrounded by two with one π bonded C═N—C (N-sp^2) and three all σ bonded C—$\ddot{N}$<(N-sp^3) neighboring carbons, respectively. It is clear that the area ratio (N-sp^2/N-sp^3) between N-sp^2 and N-sp^3 bands increases with increasing

Downloaded 23 Aug 2010 to 133.68.192.97. Redistribution subject to AIP license or copyright; see http://jap.aip.org/about/rights_and_permissions

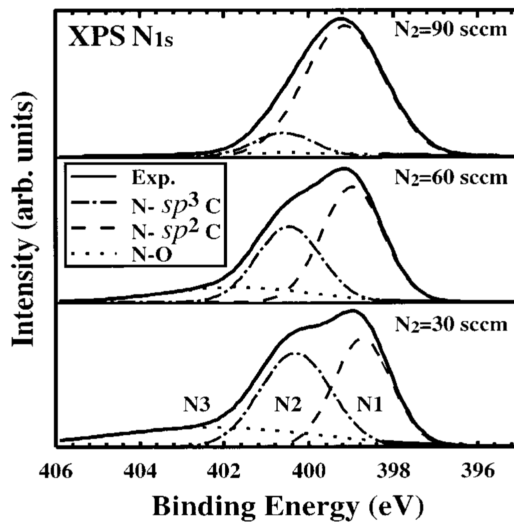

FIG. 3. The XPS N_{1s} core-level spectra of rf PECVD grown nitrogen doped a-C:H films with nitrogen flow of 30, 60, and 90 sccm. The solid lines are the measured data, and the dashed and dashed-dotted lines represent Gaussian fits.

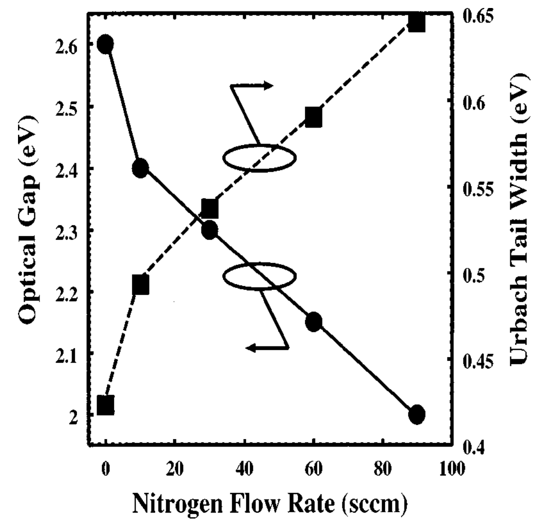

FIG. 4. The Tauc optical band gap and Urbach band tail width of rf PECVD grown nitrogen doped a-C:H films with different nitrogen flow rates.

nitrogen flow rate. Furthermore, the N-sp^2/N-sp^3 ratio sharply increases above 10 at.% nitrogen concentration (>60 sccm N_2 flow rate), and is in good agreement with the XPS results reported by Ronning *et al.*[23] Films with low concentration of nitrogen (<10 at.%) are not suitable for semiconductor device application, nitrogen doping leads to a high total energy (unstable) of configuration and an additional deep gap states and band-tail states.[21,22] With higher nitrogen incorporation in the network, the nitrogen tends to decrease the sp^3 content in a-C:H and therefore reduce the N—C coordination number.

It should be noted that there is some controversy in the interpretation of the N1 and N2 XPS peaks of CN_x. Some authors have assigned the N1 peak to nitrogen bonded to sp^3-hybridized carbon, and the N2 peak to nitrogen bonded to sp^2-coordinated carbon.[26–28] This interpretation is in contrast with that of other authors[23,29] and ours as just discussed above. Regarding the N1 peak, Harmmer *et al.* assigns as the main contribution of N1 peak to nonaromatic CN bonds with nitrogen having three σ bonded C neighbors and a localized nitrogen lone pair orbital.[30] Therefore, we suggest that the possible assignments of the respective peaks can be checked out by looking at other film properties characterized by UV-VIS, ESR, and PL. The details are discussed in the following paragraphs.

From UV-VIS spectroscopy data, the Tauc optical gap ($E_{\rm opt}$) was calculated using the Tauc equation, $[E \times \alpha(E)]^{1/2} = B \times (E - E_{\rm opt})$, where B is a constant. Urbach band tail width (E_0) was calculated using the formula $\alpha(E) = \exp[(E - E_{\rm opt})/E_0]$.[13] The variations in the $E_{\rm opt}$ and E_0 with nitrogen flow rate are shown in Fig. 4. $E_{\rm opt}$ decreases from 2.6 to 2.0 eV and E_0 increases from 424 to 646 meV with increasing nitrogen flow rate. For the nitrogen doped a-C:H films, it can be observed that both $E_{\rm opt}$ and E_0 values vary linearly with nitrogen flow rate. In general, the shape of the band tails can be obtained from B^{-1} and the Urbach band tail width, E_0, is a measure of the disorder of the films. The increase in E_0 and a decrease in B^{-1}, which decreases from 70 to 61 μeV cm with an increasing nitrogen flow rate, indicate an increase in the disorder and a broadening of the band tail within the films. According to the cluster model proposed by Robertson and O'Reilly,[13,31] a-C:H contains both sp^2 and sp^3 sites, with sp^2 sites segregated into clusters embedded in an sp^3-bonded matrix. The difference between the $\pi-\pi^*$ gap of the sp^2 sites and the $\sigma-\sigma^*$ gap of the sp^3 sites creates very strong static disorder fluctuations. This model suggests that the size of sp^2 clusters (or the disorder in the film) increases linearly with increasing nitrogen flow rate, thereby decreasing the Tauc optical gap. The incorporated nitrogen acts as a bridge atom between the clusters leading to an increase in the sp^2 cluster size.[32]

Our result concerning the change of Tauc optical gap is in good agreement with the XPS results where the N-sp^2/N-sp^3 ratio increases with increasing nitrogen flow rate. Therefore, this result supports the interpretation of our XPS N1 and N2 peaks for N-sp^2 and N-sp^3, respectively.

For the determination of optical constants and the degree of inhomogeneity from the ellipsometric measurements, we have employed a computer fitting procedure. The details of the theoretical treatment for ellipsometric measurement of an inhomogeneous film have been discussed in our previous publication.[33] In our SE data analysis, the unknown dielectric function of a-C:H is described by the model developed by Jellison and Modine based on the classical Lorentz oscillator and Tauc joint density of states,[34] which is given by

$$\epsilon_{2\rm TL}(E) = \begin{cases} \left[\dfrac{A E_0 C (E-E_g)^2}{(E^2-E_0^2)^2 + C^2 E^2} \left(\dfrac{1}{E} \right) \right] & \text{if } E > E_g, \\ 0 \quad \text{if } E \leqslant E_g, \end{cases} \tag{1}$$

where E_g is the optical band gap, E_0 is the peak transition energy, C is the broadening term, and A is the constant. The subscript TL indicates that the model is based on the Tauc joint density of states and the Lorentz oscillator; the four

Downloaded 23 Aug 2010 to 133.68.192.97. Redistribution subject to AIP license or copyright; see http://jap.aip.org/about/rights_and_permissions

TABLE II. The coefficients of the TL model $[A, E_0, C,$ and $\epsilon_1(\infty)]$, void fraction at the inner surface of *a*-C:H film (f_{vi}), and thickness of the rough layer (d_1) and *a*-C:H film (d_2) for all the samples, obtained by fitting the SE data. The 90% confidence limit are given with (±).

Sample No.	A (eV)	E_0 (eV)	C (eV)	E_g (eV)	$\epsilon(\infty)$	f_{vi}	d_1 (nm)	d_2 (nm)	δ
1	9.9 ±0.1	6.61 ±0.02	2.85 ±0.01	2.25 ±0.01	1.97 ±0.01	−0.06 ±0.02	6.4 ±0.2	1234.4 ±0.1	0.095
2	8.67 ±0.03	6.233 ±0.001	4.31 ±0.01	2.01 ±0.01	2.03 ±0.01	−0.110 ±0.001	5.38 ±0.04	1154.24 ±0.02	0.033
3	8.29 ±0.03	5.65 ±0.01	3.24 ±0.01	1.95 ±0.02	1.984 ±0.002	−0.178 ±0.02	3.93 ±0.09	1006.91 ±0.02	0.035
4	8.04 ±0.08	5.26 ±0.01	3.03 ±0.05	1.84 ±0.01	2.039 ±0.002	−0.161 ±0.009	3.23 ±0.05	802.89 ±0.02	0.015
5	12.5 ±0.2	6.57 ±0.02	4.42 ±0.04	1.74 ±0.07	1.76 ±0.01	−0.159 ±0.05	1.0 ±0.3	1165.5 ±0.2	0.093

fitting parameters E_g, E_0, C, and A are all in units of energy. The real part of the dielectric function ϵ_1 is obtained by Kramers–Kronig integration, given by

$$\epsilon_1(E)=\epsilon_1(\infty)+\frac{2}{\pi}P\int_{E_g}^{\infty}\frac{\zeta\epsilon_2(\zeta)}{\zeta^2-E^2}d\zeta, \quad (2)$$

where P stands for the Cauchy principal part of the integral and an additional fitting parameter $\epsilon_1(\infty)$ is also included. The independent unknown parameters E_g, A, E_0, C, and $\epsilon_1(\infty)$ are numerically determined by minimizing the mean squares deviation (δ^2) with a regression program.[33]

A four-phase structure (air/rough surface layer with thickness of d_1/inhomogeneous *a*-C:H film with thickness of d_2/substrate) has been used in the simultaneous fitting of measured parameters Δ and Ψ of SE. The rough layer on the surface was modeled as an effective mixture of 50% *a*-C:H and 50% void. Inhomogeneity of a film results from the nonuniform packing density of the film which is usually expressed by the volume fraction of void f_v. In our fitting analysis f_v is linearly varied from $f_{vo}=0$ at the outer surface of the film to f_{vi} at the inner surface. This simplifies the calculation than considering the refractive index varying along the thickness of the film since f_v is a function of distance only while refractive index is a function of both distance and wavelength. However, it should be noted that our assumption of f_v varying from zero at the outer surface to f_{vi} at the inner surface is only for the sake of obtaining the distribution of dielectric function along the depth of the film by fitting to ellipsometric data and shows only relative variation in the void fraction along the thickness of the film. Table II shows the best fit model parameters used in the simulation of cos Δ and tan Ψ spectra. As shown in Table II. the optical gap (E_g) gradually decreases from 2.25 to 1.74 eV as the nitrogen concentration increases from 0 to 21.2 at.%. The values of E_g obtained by SE analysis are different from those of the E_{opt} obtained by UV-VIS analysis because the definition of the optical gap, E_g and E_{opt}, is different in the two models. However, both results show the same trend of decreasing optical band gap with increasing nitrogen flow rate. It is reported that nitrogen incorporation in *a*-C:H leads to graphitization when deposited with standard PECVD system.[35,36] The incorporated nitrogen acts as a bridge atom between the clusters and this leads to the increase of the sp^2 clusters size,[32,37] thereby decreasing the optical band gap according to the cluster model.

Figure 5 shows the variation in the refractive index n (top) and extinction coefficient k (bottom) spectra at the surface of the samples, calculated using the film structure parameters as listed in Table II. While k gradually increases with nitrogen concentration, n first remains almost the same at low nitrogen concentration after which it increases with a further increase in nitrogen concentration. The increase in k with increased nitrogen incorporation is due to the graphitization effect which decreases the optical gap resulting in higher k. The increase in n with increased nitrogen incorpo-

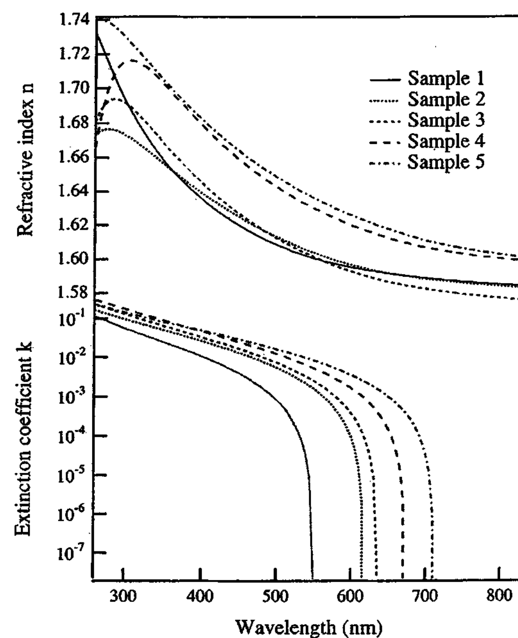

FIG. 5. Variation of the refractive index n (top) and extinction coefficient k (bottom) spectra at the surface of the samples over the wavelength range 300–830 nm.

Downloaded 23 Aug 2010 to 133.68.192.97. Redistribution subject to AIP license or copyright; see http://jap.aip.org/about/rights_and_permissions

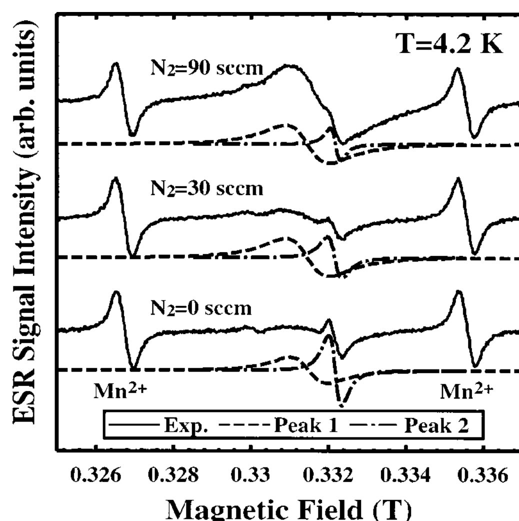

FIG. 6. The 4.2 K ESR spectra of rf PECVD grown nitrogen doped *a*-C:H films with nitrogen flow of 0, 30, and 90 sccm. The solid lines are the measured data, and the dashed and dashed-dotted lines represent Lorentzian fits.

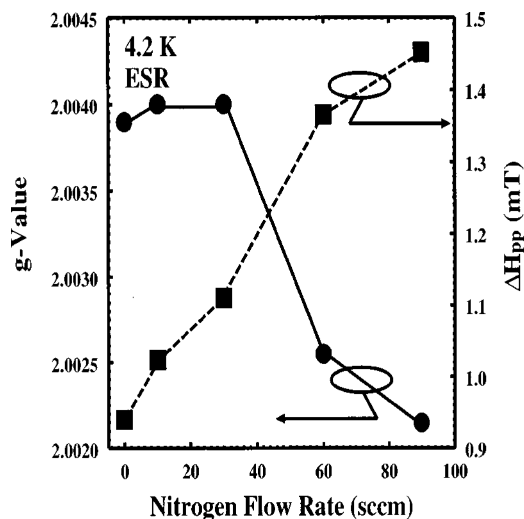

FIG. 7. The dependence of the g value and ESR peak-to-peak linewidth ΔH_{pp} on nitrogen flow rate.

ration is probably due to the removal of hydrogen and formation of C—N and C═N bonds in the film. For all the films, the refractive index at the film–substrate interface is found to be the highest and it gradually decreases towards the surface. Silicon is a crystalline substrate and it is likely that it will influence the formation of a dense carbon film with high sp^3/sp^2 ratio near its surface leading to higher value of n.[38] Therefore, we believe that the index gradient is partly due to the variation in the sp^3/sp^2 ratio and partly due to the variation in the void fraction along the thickness of the film.

A complex ESR single resonance spectra are observed at 4.2 K as shown in Fig. 6. The ESR resonance spectra can be analyzed quantitatively using a computer to reproduce the data as a sum of peaks with the 100% Lorentzian shapes. The resonance is composed of two peaks, centered at around 0.331 (peak 1) and 0.332 T (peak 2), respectively. The peaks 1 and 2 are associated with carbon and quartz substrate, respectively. It should be noted that the peak 1 is not easily saturated by the incident microwave power and this result indicates that the resonance is due to a delocalized ESR center rather than a localized ESR center.

The effect of nitrogen doping on the ESR parameters of *a*-C:H film is shown in Fig. 7. A rapid decrease in the g value from 2.0039 to 2.0025 is observed which is accompanied by a rapid rise in the peak-to-peak linewidth (ΔH_{pp}) from 1.1 to 1.4 mT as the nitrogen flow increases from 30 to 60 sccm. However, these results are in contrast to those of others where they reported a decrease in ΔH_{pp} as the sp^2 content in the film increases and associated it with the greater delocalization of the unpaired electrons as the cluster size increases.[39] Several authors attributed the Lorentzian line shape and ΔH_{pp} narrowing of the *a*-C:H ESR line to exchange interaction between the spins (exchange narrowing).[40–42] Recently, Barklie *et al.*[42] have observed an increase in ΔH_{pp} in *a*-C:H deposited by PECVD with negative self-bias voltage below 100 V and interpreted the results in terms of dipolar contribution and unresolved hydrogen hyperfine interactions based on the mixture of Lorentzian and Gaussian shapes. The question is, therefore, why does the ΔH_{pp} increase? We suggest that the increase in ΔH_{pp} of our films with increase in nitrogen flow rate is due to the reason that the spins are no longer localized at a single C—N cluster but are able to tunnel to neighboring C—N clusters based on the unsaturation behavior of peak 1 and the aforementioned discussion.

Figure 8 shows the PL spectra of undoped and nitrogen doped (nitrogen flow 90 sccm) *a*-C:H films with the spectral peak intensities being normalized to the maximum peak intensity. The spectrum shows mainly two peaks at 1.7 and 2.4 eV. Although *a*-C:H exhibits strong room temperature PL in the visible region, the appropriate mechanism of PL is not well understood yet. However, the PL peak at 1.7 eV is related to electronic transition from conduction band to valence band through localized recombination centers. Also,

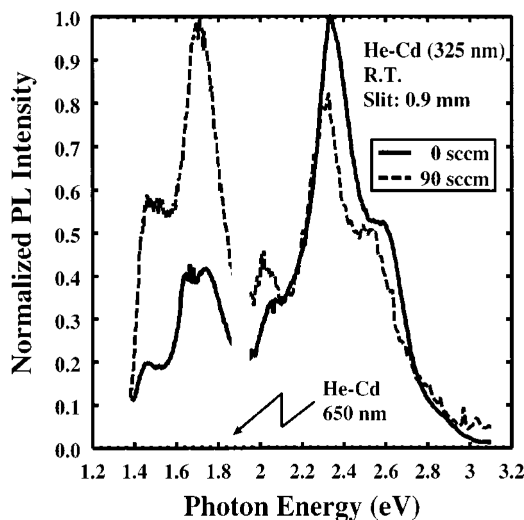

FIG. 8. The PL spectra of rf PECVD grown nitrogen doped *a*-C:H films with nitrogen flow of 0 and 90 sccm.

Downloaded 23 Aug 2010 to 133.68.192.97. Redistribution subject to AIP license or copyright; see http://jap.aip.org/about/rights_and_permissions

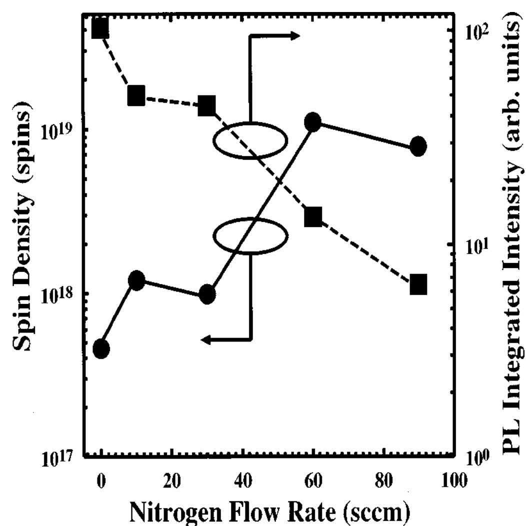

FIG. 9. The dependence of the ESR spin density, N_s, and PL integrated intensity between 2 to 3 eV band on nitrogen flow rate.

the PL peak at 2.4 eV can be explained by electronic transition from conduction band edge to valence band edge. The PL emission intensity ratio between 1.7 and 2.4 eV ($I_{1.7}/I_{2.4}$) increases with increasing nitrogen flow rate. It should be noted that the overall PL spectral shape of the films with and without nitrogen is same.

In comparison with Fig. 4, it is noteworthy that the difference between the PL emission peak energy and the optical absorption edge is as large as 0.2 eV for the film deposited with nitrogen flow of 0 sccm and is described as the Stokes shift. On the other hand, we observe as large as 0.2 eV anti-Stokes shift from the film deposited with nitrogen flow of 90 sccm. The difference between the optical absorption and PL emission processes was discussed in our previous study based on the sp^2 bonded cluster size and its distribution model for the *a*-C:H thin films.[9] According to this, the PL/ emission strongly reflects the largest cluster size, whereas, the Tauc optical gap represents the average value of cluster size distribution.

The ESR spin density and the total luminescence efficiency are shown in Fig. 9. The total luminescence efficiency was obtained by calculating the integrated intensity between 2 to 3 eV of the PL spectra. The ESR spin density initially rises with the incorporation of nitrogen and then rapidly increases between the nitrogen flow rates of 30 and 60 sccm. The rapid increase in ESR spin density and an increase in ΔH_{pp} just mentioned indicate that a large structural modification has occurred. The loss of PL integrated intensity arises from nonradiative recombination. We have found a strong correlation between PL integrated intensity (or efficiency) and ESR spin density (residual defect density) where there is a trend of decreasing PL integrated intensity with increasing ESR spin density. The detailed PL mechanism associated with the ESR spin density for the *a*-C:H films has been discussed elsewhere.[9]

Considering the UV-VIS absorption and PL spectra, a refined electronic state density of undoped and nitrogen doped *a*-C:H is presented in Figs. 10(a) and 10 (b), respectively. In this model, we consider the nitrogen lone pair band (LP)[43,44] and the Urbach tail energy, which was previously discussed, is assigned to the edge of π^* antibonding conduction band. The Urbach tail energy increases by nitrogen incorporation. According to the model for the film deposited without nitrogen, the energy gap $E_{\pi-\pi^*}$, between bonding π valence band and π^* conduction band, corresponds to the 2.4 eV PL emission. The energy gap $E_{\mathrm{DB}-\pi^*}$, between π valence band and extended π^* conduction band (DB) due to defects, corresponds to 1.7 eV PL emission. As mentioned, the nitrogen incorporation does not affect the PL overall spectral shape. If a crystal becomes disordered involving *a*-C:H, it will lose the *k*-selection rule in the interband optical transitions. Therefore, the interband optical transitions forbidden by *k*-selection rule can also be realized and will lead to a broad PL emission band in *a*-C:H. To explain the PL phenomenon in our films, the origin of 2.4 eV PL emission is changed from $E_{\pi-\pi^*}$ to $E_{\mathrm{DB/LP}-\sigma^*}$ between σ^* conduction band and the enhanced DB/LP state density due to both defects and LP induced by nitrogen incorporation. The origin of 1.7 eV PL emission is basically unchanged, however, the

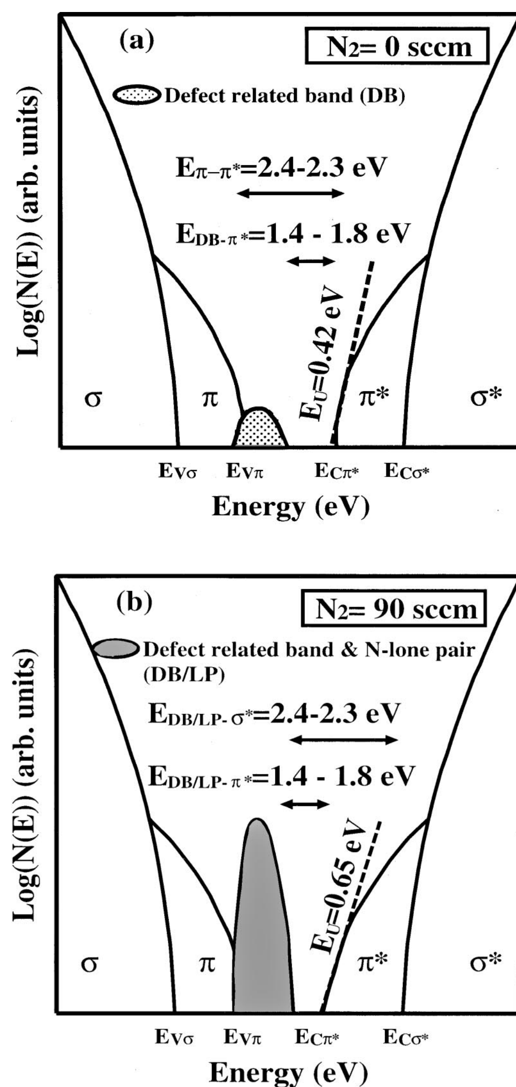

FIG. 10. A model of the electron state density of rf PECVD grown nitrogen doped *a*-C:H film.

Downloaded 23 Aug 2010 to 133.68.192.97. Redistribution subject to AIP license or copyright; see http://jap.aip.org/about/rights_and_permissions

state density of this band is enhanced by defects and LP. Therefore, the notation of energy gap is changed from $E_{DB-\pi*}$ to $E_{DB/LP-\pi*}$.

IV. SUMMARY AND CONCLUSION

In summary, a detailed characterization of nitrogen doped *a*-C:H thin films deposited with different nitrogen concentration by rf PECVD has been carried out by spectroscopic measurements. The nitrogen concentration varied up to 21.2 at.% in our films.

Raman spectroscopy and FTIR absorption reveal an increase of sp^2-bonded carbon or a change in sp^2 domain size with increasing nitrogen flow rate. Furthermore, the C═C sp^2 stretching vibrations of olefinic or conjugated carbon chains were clearly observed. It has been shown that the chemical environment of the nitrogen atoms in the deposited amorphous carbon network gradually changes from nitrogen atoms surrounded by three (σ bonded) to two (π bonded) neighboring carbons with increasing nitrogen flow rate. Nitrogen incorporation decreases the Tauc optical gap from 2.6 to 2.0 eV. The consistency in the relative changes in the XPS N-sp^2 and N-sp^3 peak areas and the variation of the Tauc optical gap with increasing nitrogen concentration signify an increase of the sp^2 bonded carbon cluster size. The SE analyses reveal gradual decrease in the optical gap, E_g, and increase in the extinction coefficient, k, with increasing nitrogen flow rate due to the increase in sp^2 bonded cluster size. Refractive index, n, first remains same and then increases with further increase in nitrogen flow rate. For all the samples, n is found to be highest at the film–substrate interface which gradually decreases towards the film surface. The ESR spin density and the ΔH_{pp} increases sharply with increasing nitrogen flow rate, especially above N_2/CH_4 gas ratio of 1. We suggest that the increase in ΔH_{pp} of our films with an increase in nitrogen concentration is because the spins are no longer localized at a single C—N cluster but able to tunnel to neighboring C—N clusters based on the unsaturation behavior. There exits a strong correlation between PL integrated intensity and ESR spin density where there is a trend of decreasing PL integrated intensity with increasing ESR spin density. Finally, a refined model of electronic density of states has been proposed which includes the nitrogen LP band and defect related band for the films deposited both without and with nitrogen, based on the optical characteristics of the films obtained form UV-VIS and PL analyses and defect density study by ESR.

It is evident that the nitrogen incorporation into *a*-C:H network plays a major role in governing the optical characteristics, the bonding network, and the defects. Thus, successful control of nitrogen incorporation into *a*-C:H will help realize efficient electronic devices, such as a solar cell.

ACKNOWLEDGMENTS

This work was partly supported by the Japan Society for the Promotion of Science under the program ''Research for the Future.''

[1] M. Yoshimi, H. Shimizu, and K. Hattori, Optoelectron., Devices Technol. **7**, 69 (1992).
[2] S. B. Kim and J. F. Wager, Appl. Phys. Lett. **53**, 1880 (1988).
[3] H. C. Tsai and D. B. Bogy, J. Vac. Sci. Technol. A **5**, 3287 (1987).
[4] H. A. Yu, Y. Kaneko, S. Yoshimura, and S. Otani, Appl. Phys. Lett. **68**, 547 (1996).
[5] K. M. Krishna, T. Soga, T. Jimbo, and M. Umeno, Carbon **37**, 531 (1999).
[6] H. Yoenhara and C. Pac, Thin Solid Films **270**, 108 (1995).
[7] K. Murata, S. Ito, K. Takahashi, and B. M. Hoffman, Appl. Phys. Lett. **68**, 427 (1996).
[8] K. M. Krishna, Y. Nukaya, T. Soga, T. Jimbo, and M. Umeno, Appl. Phys. Lett. **77**, 1472 (2000).
[9] Y. Hayashi, K. Hagimoto, H. Ebisu, M. K. Kalaga, T. Soga, M. Umeno, and T. Jimbo, Jpn. J. Appl. Phys., Part 1 **39**, 4088 (2000).
[10] S. R. P. Silva, B. Rafferty, G. A. J. Amaratunga, J. Schwan, D. F. Franceschini, and L. M. Brown, Diamond Relat. Mater. **5**, 401 (1996).
[11] M. Zhang, Y. Nakayama, and S. Harada, J. Appl. Phys. **86**, 4971 (1999).
[12] A. Ilie, O. Harel, N. M. J. Conway, T. Yagi, J. Robertson, and W. I. Milne, J. Appl. Phys. **87**, 789 (2000).
[13] R. A. Street, *Hydrogenated Amorphous Silicon* (Cambridge University Press, Cambridge, UK, 1991), p. 86.
[14] J. H. Kafuman and S. Metin, Phys. Rev. B **39**, 13053 (1989).
[15] Z.-M. Ren, Y.-C. Du, Y. Qiu, J.-D. Wu, Z.-F. Ying, X.-X. Xiong, and F.-M. Li, Phys. Rev. B **51**, 5274 (1995).
[16] R. Nemanich and S. Solin, Phys. Rev. B **20**, 392 (1979).
[17] J. Schwan, S. Ulrich, V. Batori, H. Ehrhardt, and S. P. R. Silva, J. Appl. Phys. **80**, 440 (1996).
[18] A. R. Zanatta and I. Chambouleyron, Phys. Rev. B **48**, 4560 (1993).
[19] F. Demichelis, X. F. Rong, S. Schreiter, A. Tagliaferro, and C. DeMartino, Diamond Relat. Mater. **4**, 361 (1995).
[20] J. Shiao and W. Hoffman, Thin Solid Films **283**, 145 (1996).
[21] P. L. Sitch, T. Köhler, G. Jungnickel, D. Porezag, and T. Frauenheim, Solid State Commun. **100**, 549 (1996).
[22] P. Stumm, D. A. Drabold, and P. A. Fedders, J. Appl. Phys. **81**, 1289 (1997).
[23] C. Ronning, H. Feldermann, R. Merk, H. Hofsäss, P. Reinke, and J.-U. Thiele, Phys. Rev. B **58**, 2207 (1998).
[24] S. Kobayashi, S. Nozaki, H. Morisaki, S. Fukui, and S. Masaki, Thin Solid Films **281**, 289 (1996).
[25] H. Xin, C. Lin, S. Zhu, S. Zou, Z. Shi, and P. L. F. Hemment, Nucl. Instrum. Methods Phys. Res. B **103**, 309 (1995).
[26] D. Marton, K. Boyd, A. H. Al-Bayati, S. S. Todorov, and J. W. Rabalais, Phys. Rev. Lett. **73**, 118 (1994).
[27] N. Hellgren, M. P. Johansson, E. Broitman, L. Hultman, and J. E. Sundgren, Phys. Rev. B **59**, 5162 (1999).
[28] S. Souto, M. Pickholz, M. C. dos Santos, and F. Alvarez, Phys. Rev. B **57**, 2536 (1998).
[29] M. L. De Giorgi *et al.*, Appl. Surf. Sci. **127**, 481 (1998).
[30] P. Harmmer, N. V. Victoria, and F. Alvarez, J. Vac. Sci. Technol. A **18**, 2277 (2000).
[31] J. Robertson and E. P. O'Reilly, Phys. Rev. B **35**, 2946 (1987).
[32] F. Demichelis, Y. Lui, X. Rong, S. Schreiter, and A. Tagliaferro, Solid State Commun. **95**, 475 (1995).
[33] M. M. Rahman, G. Yu, K. Murali Krishna, T. Soga, J. Watanabe, T. Jimbo, and M. Umeno, Appl. Opt. **37**, 691 (1998).
[34] G. E. Jellison, Jr. and F. A. Modine, Appl. Phys. Lett. **69**, 371 (1996).
[35] O. Amir and R. Kalish, J. Appl. Phys. **70**, 4958 (1991).
[36] J. Schwan, W. Dworschak, K. Jung, and H. Ehrhardt, Diamond Relat. Mater. **3**, 1034 (1994).
[37] Y. Hayashi, H. Ebisu, M. K. Kalaga, T. Soga, M. Umeno, and T. Jimbo, Diamond Relat. Mater. (in press).
[38] M. M. Rahman, G. Yu, H. Ebisu, T. Soga, T. Jimbo, and M. Umeno, J. Appl. Phys. **88**, 4634 (2000).
[39] J. Robertson, Adv. Phys. **35**, 317 (1986).
[40] G. Fusco, A. Tagliaferro, W. I. Milne, and J. Robertson, Diamond Relat. Mater. **6**, 783 (1997).
[41] R. C. Barklie, M. Collins, J. Cunniffe, and S. R. Silva, Diamond Relat. Mater. **7**, 864 (1998).
[42] R. C. Barklie, M. Collins, and S. R. Silva, Phys. Rev. B **61**, 3456 (2000).
[43] S. Souto, M. Pickholz, M. C. dos Santos, and F. Alvarrez, Phys. Rev. B **57**, 2536 (1998).
[44] T. Katsuno, H. Habuchi, T. Iwasaki, T. Itho, and S. Nonomura, Mater. Res. Soc. Symp. Proc. **593**, 499 (2000).

Downloaded 23 Aug 2010 to 133.68.192.97. Redistribution subject to AIP license or copyright; see http://jap.aip.org/about/rights_and_permissions